Robotics-Assisted Mirror Rehabilitation Therapy: A Therapist-in-the-Loop Assist-as-Needed Architecture†‡

Mahya Shahbazi, *Student Member, IEEE,* S. Farokh Atashzar, *Student Member, IEEE,*
Mahdi Tavakoli, *Member, IEEE,* Rajni V. Patel, *Life Fellow, IEEE*

Abstract—This paper presents a Therapist-in-the-Loop (TIL) framework for robotics-assisted mirror rehabilitation integrated with *adaptive* Assist-as-Needed Therapy (ANT) that is adjusted based on the impairment level of the patient's affected limb. The framework which is designed for patients with hemiparesis and/or hemispatial neglect, uses a Patient's Functional Limb (PFL) as the medium to transfer therapeutic training from the therapist to the Patient's Impaired Limb (PIL). This allows the patient to use his/her functional limb to adjust the desired trajectory generated by the therapist if the trajectory is painful or uncomfortable for the PIL. In order to realize the adaptive patient-targeted therapy, two motor-function assessment metrics, *Performance Symmetry* and *Level Of Guidance* are proposed, providing real-time, task-independent and objective assessment of the PIL's motor deficiency. An adaptation law is also presented to adjust the intensity of the therapy delivered to the patient in real-time and based on the aforementioned estimation of the impairment level of the PIL. Closed-loop system stability has been investigated in the presence of communication delays to facilitate tele / in-home rehabilitation. For this purpose, a combination of the Circle Criterion and the Small-Gain Theorem has been applied to account both for communication time delays and the *time-varying* adaptive ANT. Results of experiments to investigate the performance of the proposed framework are reported.

LIST OF ACRONYMS

PIL: Patient's Impaired Limb, **PFL:** Patient's Functional Limb, **TIL:** Therapist-in-the-Loop, **MT:** Mirror Therapy, **ANT:** Assist-as-Needed Therapy, **ANMT:** Assist-as-Needed Mirror Therapy, **GVF:** Guidance Virtual Fixture, **SPR:** Strictly Positive Real, **TCT:** Therapist-Commanded Trajectory, **PS:** Performance Symmetry, **MS:** Movement Smoothness, **TPL:** Total Path Length, **LOG**: Level Of Guidance.

M. Shahbazi and S.F. Atashzar are with Canadian Surgical Technologies and Advanced Robotics (CSTAR), and with the Department of Electrical and Computer Engineering, Western University, London, ON, Canada. They were also visiting research scholars at the University of Alberta, Edmonton, AB, Canada (email: mshahba2@uwo.ca, satashza@uwo.ca). M. Tavakoli is with the Department of Electrical and Computer Engineering, University of Alberta, Edmonton, AB, Canada (email: mahdi.tavakoli@ualberta.ca). R.V. Patel is with CSTAR, the Department of Electrical and Computer Engineering, the Department of Surgery and the Department of Clinical Neurological Sciences, Western University (email: rvpatel@uwo.ca).

I. INTRODUCTION

Annually 15 million people worldwide suffer from stroke. With a survival rate of about 70%, stroke is known to be a major leading cause of long-term disabilities and severe impairments [1], [2]. The significant number of patients recovering from stroke, in addition to other neurological disorders, has led to a growing need for rehabilitation services to induce neuroplasticity in patients. Neuroplasticity is referred to as the reorganization ability of the brain by developing new neural connections through sensory input, experience, and learning, which allows the brain's neurons to compensate for injury and disease [3]. Achieving brain neuroplasticity from rehabilitation therapy is a labor-intensive process, which necessitates not only a therapist's expertise and knowledge, but also reproducible movements and stereotyped exercises. This has led to a paradigm shift towards robotics-assisted rehabilitation therapy, offering novel recovery-assessment approaches along with patient-targeted rehabilitation therapies [4], [5].

Robotics-assisted mirror therapy, a recent form of robotic rehabilitation, has received a great deal of attention during the past decade [6] . This type of therapy is particularly useful for patients with hemiparesis [7], the most common movement impairment. Hemiparesis refers to one-sided weakness and affects about 80% of stroke survivors [8]. Effectiveness of mirror therapy has been also shown for patients suffering from unilateral neglect after stroke [9]. Unilateral neglect, also known as hemispatial neglect, is a symptom of a brain damage in which the person experiences a deficit in attention to and awareness of one side of his/her body and anything in the external world on the same side. A patient with this neurological condition is unable to perceive and process stimuli on that side of the body or the environment, while that inability is not due to a lack of sensation [10].

During robotics-assisted mirror therapy, motions of the Patient's Functional Limb (PFL) are mirrored through a telerobotic medium to the Patient's Impaired Limb (PIL), promoting the functional recovery of the impaired/affected limb through the spatial coupling effect between the two limbs. This results from the tendency of one limb to adopt the spatial features of the other limb [11], [12], [13]. Through mirror-symmetric (or any other coordinated bimanual) movement pattern for the two limbs in mirror therapy, the unimpaired hemisphere of the brain interacts with the impaired hemisphere, thereby inducing reorganization of the motor cortex networks and facilitating cortical neuroplasticity [14], [11]. The effectiveness of mirror-symmetric *bimanual* therapy has been shown in comparison with conventional *unimanual* therapy to result in an increase in the functional ability as well
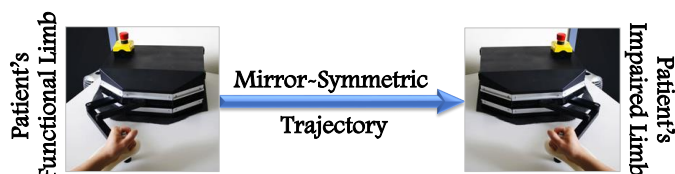
Fig. 1. The overall scheme of the conventional robotics-assisted MT.

as a decrease in movement completion times for the PIL [15]. Mirror therapy has also been shown to be effective in terms of improving the accuracy, active range of motion, dexterity and grip strength of the limb [16], [17], [18], [19].

Existing robotics-assisted mirror-therapy systems, such as MIME [20], provide a unilateral Single-Master/Single-Slave (SM/SS) telerobotic framework in order for the PIL to move in accordance with the mirror-image motions of the PFL. This gives patients some level of control over the therapy through the involvement of their functional limb. However, due to the inherently restrictive structure of SM/SS systems [21], the PIL interacting with the slave robot can only receive commands from the PFL interacting with the master robot. This means that a therapist cannot be directly involved in the rehabilitation loop to apply corrective movements or to monitor/assess the PIL performance through haptic feedback. Fig. 1 shows the overall scheme of a conventional robotics-assisted mirror therapy system. Presence of an expert in the loop of the therapy can play an essential role in promoting the patient's functional recovery. Based on a recent study published [22], haptics-based interaction with a partner when learning a motor task considerably enhances the motor skills compared to when practicing the task alone for the same duration. Therefore, haptics-based interaction of a therapist with a patient can be effective not only because of the therapist's knowledge and expertise, but also due to his/her positive effect on the patient's learning curve as a result of the interaction. Capitalizing on the impact of therapist-patient haptics-based interaction, in this paper a Therapist-In-the-Loop (TIL) framework is proposed for robotics-assisted mirror therapy based on a *supervised trilateral* telerobotic system integrated with adaptive Assist-as-Needed Therapy (ANT) that is adjusted based on the impairment and disability level of the patient's affected limb. The overall scheme of the proposed framework is shown in Fig. 2. The proposed architecture offers the following innovations:

(1) Therapist-in-the-loop MT,

(2) PFL-mediation,

(3) Haptic feedback to the therapist,

(4) Adaptive GVF,

(5) Task-independent and patient-specific motor-function assessment,

(6) Closed-loop stability analysis,

which are discussed below.

The architecture establishes a mirroring behavior between the patient's two limbs, while the desired trajectories are provided by a therapist supervising the therapy. This is expected to enhance the treatment by bringing the therapist's expertise directly into the treatment. The framework is designed such that the trajectories desired for the PIL are commanded by the therapist through the PFL, where the PFL has the ability to modify/update the trajectory. Therefore, having the PFL as a medium between the therapist and the PIL, the therapist-commanded trajectories can be conditioned before being passed on to the PIL. Benefiting from the patient's proprioceptive knowledge and self-awareness of workspace limitations, the proposed PFL-mediated approach enables the patient to modify the therapist-commanded trajectories in order to avoid painful/uncomfortable maneuvers for the PIL, of which the therapist may not be aware. Based on how closely the therapist-commanded trajectories are followed by the PIL, which may have been modified by the PFL in the interest of patient safety and comfort, the system also provides the therapist with haptic feedback. This would allow the therapist to better decide on the intensity of the therapy administered to and acceptable for the patient.

The framework also provides the patient with *adaptive* Assist-as-Needed Therapy (ANT) using a time-varying Guidance Virtual Fixture (GVF). A GVF is a suitable approach for providing kinesthetic guidance along desired trajectories [23]. In this paper, the intensity/forcefulness of the GVF is proposed to be adaptively adjusted based on the patient's impairment/performance level perceived during the therapy.

For this purpose, benefiting from the presence of the PFL in the therapy loop, a novel performance assessment framework (called *performance symmetry* (PS)) is proposed for mirror therapy, based on which the adaptive GVF is adjusted in real time. PS provides a relative quantifiable assessment of the PIL performance by comparing it to the PFL performance as the patient's gold standard. Unlike the absolute assessment metrics currently available in the literature [5], [24], the proposed PS metric takes the performance level of the PFL into account for each patient when assessing the PIL performance for the same patient. Consequently, the quantified assessment results will be more objective, easier to interpret, and adjusted to the inevitable intra-patient variability in motor deficiency.

In addition to PS, another metric is also proposed based on the *Level Of Guidance* (LOG) provided to the PIL during the treatment. Using this metric in parallel with other performance metrics enables the assessment process to distinguish between performance improvements due to the patient's functional recovery vs. those due to the GVF-based assistance to the patient during the treatment. The aforementioned PS and LOG metrics, along with two other metrics from the literature, are used to develop an adaptation law for updating the adaptive ANT based on the impairment level of the PIL.

As there are three sets of local sub-systems (PIL, PFL and therapist), globally interacting through a trilateral telerobotic architecture, stability of the closed-loop system should be investigated in order to guarantee system stability. For this purpose, a combination of the Circle Criterion and the Small-Gain Theorem is applied and a set of sufficient stability conditions is derived. The proposed stability analysis addresses instabilities caused by communication delays between the therapist and the patient. This facilitates the case of haptics-enabled bilateral tele-rehabilitation, which is suitable for applications such as in-home rehabilitation [25], [26]. Incorporating the

Circle Criterion into the Small-Gain Theorem, the proposed procedure also addresses extra stability-analysis challenges raised by the integration of the time-varying nonlinear GVF element into the delayed closed-loop system.

Through the proposed trilateral framework, the patient benefits from an enhanced motor-recovery process as a result of integrating the following characteristics: (a) the cross-cortex coupling effect between limbs induced by the mirror therapy; (b) the expertise and direct supervision of, along with the haptic feedback delivered to, the therapist in the loop over the treatment to provide appropriate corrective movements; (c) the supervision/impact of the patient over the treatment through the PFL-mediated feature, which guarantees the patient's safety and comfort by avoiding the application of excessive pressure and pain on the PIL; and (d) active involvement of the patient in the treatment through the adaptive GVF-based ANT.

The rest of this paper is organized as follows: Section II presents the proposed architecture. Section III discusses the metrics proposed and the adaptation law developed for ANT. Section IV presents the closed-loop stability of the system in the presence of communication delays. Experimental results are given in Section V, and Section VI concludes the paper.

II. THE PROPOSED FRAMEWORK

A. Architecture for the PIL/robot interaction

In order for the PIL to undergo mirror therapy, its desired position $x_{des,PIL}$ is defined to be the mirror image of PFL's position, x_{PFL}, as follows:

$$x_{des,PIL}(t) = \beta \cdot x_{PFL}(t) \tag{1}$$

where $\beta = diag(\beta_1,...,\beta_n)$ refers to the mirroring matrix, accommodating for the mirroring effect between the functional and the impaired limb across the sagittal plane; the subscript n indicates the number of Degrees of Freedom (DOF). Depending on the mirroring plane, β_i $(i = 1, 2, \cdots, n)$, which is the mirroring coefficient for the ith DOF, can be set to either +1 or -1. For example, for mirroring along the x-axis, β_1 will be set to -1, while β_i $(i \neq 1)$ will be set to +1 in order to accommodate for the same-directional/parallel trajectories along other axes. By setting all the elements of the mirroring matrix to +1, the framework can be used for bilateral parallel therapy, which has also been shown to be effective in inducing neuroplasticity [6].

In order to provide the PIL with an assist-as-needed therapy to *actively* engage the patient in the treatment process, an adaptive GVF is proposed, the stiffness of which can be adaptively adjusted according to the impairment/disability level of the PIL. The higher level of impairment the PIL shows, the more strict and enforcing the GVF becomes to provide the patient with a higher level of assistance. The GVF is designed such that if the PIL remains within a specific range of its desired trajectory, i.e., inside a specific spherical volume centered at the desired trajectory point $x_{des,PIL}$, no GVF force will be applied to it. However, if the deviation error between the PIL and the mirror image of the PFL (the desired trajectory for PIL) exceeds a certain threshold, the GVF will apply force to the PIL in order to assist the PIL with accomplishing the trajectory. The allowable range of the deviation error is set to

be up to R_{GVF}. Exceeding the allowable range of position error, i.e., $|x_{des,PIL} - x_{PIL}| > R_{GVF}$, will cause the PIL to receive the following GVF force:

$$F_{GVF,PIL}(t) = K_{GVF,PIL}(t)(x_{des,PIL}(t) - x_{PIL}(t)) \tag{2}$$

where $K_{GVF,PIL}(t) \in [\kappa_{min}, \kappa_{max}]$ refers to the adaptive stiffness of the GVF, to be adjusted according to the impairment level of the PIL, the design of which including the patient's motor-function assessment is discussed in Section III. κ_{min} and κ_{max} indicate some positive lower and upper bounds to be considered in the design procedure for $K_{GVF,PIL}$. It should be noted that various motor-function assessment metrics, including but not limited to movement accuracy, motion smoothness, movement velocity and grip strength, can be used in order to design the variation profile of the adaptive GVF's stiffness.

In order for the patient to transparently feel the desired GVF force applied by the robot on his/her PIL, it is required to have:

$$F_{PIL}(t) = -F_{GVF,PIL}(t) \tag{3}$$

where F_{PIL} refers to the force applied by the PIL to its corresponding robot. Note that the minus sign is to account for the direction of forces, i.e., applied by the robot to the PIL or vice versa. However, as will be discussed in Section IV, similar to any other telerobotic system [27], ensuring closed-loop stability may degrade the system transparency and performance. Thus, to guarantee closed-loop stability in the presence of communication delays, a modified impedance surface is defined as the desired closed-loop system at the PIL robot, through which the GVF force $F_{GVF,PIL}$ is applied to the PIL by its corresponding robot:

$$F_{PIL}(t) = -F_{GVF,PIL}(t)+ \\ M_{\vartheta,PIL} \cdot \ddot{x}_{PIL}(t) + B_{\vartheta,PIL} \cdot \dot{x}_{PIL}(t) + K_{\vartheta,PIL} \cdot x_{PIL}(t) \tag{4}$$

where $M_{\vartheta,PIL}$, $B_{\vartheta,PIL}$ and $K_{\vartheta,PIL}$ stand for mass, damping and stiffness, respectively, to be used as the local control parameters at the PIL robot. From the performance viewpoint, the control parameters are desired to be set to zero, which results in $F_{PIL}(t) = -F_{GVF,PIL}(t)$ as in (3). However, it will be shown in Section IV how positive values for these parameters will contribute to closed-loop stability in the presence of communication time delay between the therapist and the patient in order to facilitate the case of tele and in-home rehabilitation.

B. Architecture for the PFL/robot interaction

The architecture at the PFL robot is designed such that the PFL receives commands (desired trajectories) from the therapist, but is able to deviate from them. This PFL-mediated platform allows the patient to alter the therapist-commanded trajectory, if the trajectories are felt to be painful or uncomfortable for the PIL. To realize this goal, a position-error impedance surface is designed for the PFL:

$$F_{PFL,des}(t) = M_{des,PFL}(\ddot{x}_T^*(t) - \ddot{x}_{PFL}(t))+ \\ B_{des,PFL}(\dot{x}_T^*(t) - \dot{x}_{PFL}(t)) + K_{des,PFL}(x_T^*(t) - x_{PFL}(t)) \tag{5}$$

where x_{PFL} indicates the trajectory generated by the PFL and x_T^* refers to the mirror image of the therapist-commanded trajectory. Note that since the PIL will move based on the
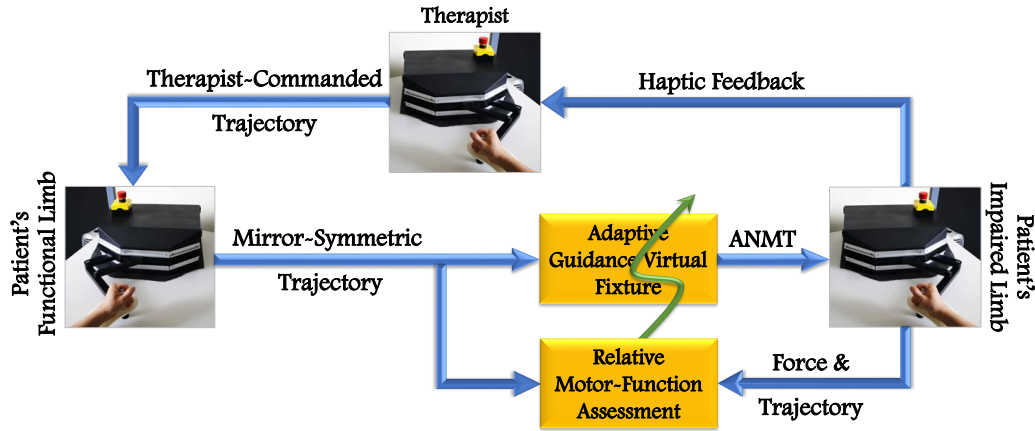
Fig. 2. The overall scheme of the supervised trilateral telerobotic framework proposed for Assist-as-Needed Mirror Therapy (ANMT).

mirror-image of the PFL, while the therapist will provide the trajectory desired for the PIL, the PFL should receive the mirror-symmetric image of the trajectory commanded for the PIL by the therapist, i.e., to receive $x_T^* = \beta \cdot x_T$, where β indicates the mirroring matrix. $M_{des,PFL}$, $B_{des,PFL}$ and $K_{des,PFL}$ refer to the desired mass, damping and stiffness, respectively, through which the PFL can alter the desired trajectories received from the therapist in the interest of safety and comfort. In addition, $F_{PFL,des}$ stands for the desired force applied by the robot to the PFL as a result of interaction with the therapist. In order for the PFL to receive $F_{PFL,des}$, it is desired to have:

$$F_{PFL} = -F_{PFL,des}, \tag{6}$$

where F_{PFL} indicates the force applied by the PFL to the robot. Consequently, and based on the desired impedance surface defined in (5), the position of the functional limb will be:

$$X_{PFL}(s) = \frac{F_{PFL}(s)}{Z_{des,PFL}(s)} + \beta \cdot X_T(s) \tag{7}$$

where $Z_{des,PFL}(s) = M_{des,PFL}s^2 + B_{des,PFL}s + K_{des,PFL}$. Here, s indicates the Laplace transform variable. Thus, the PFL can follow the mirrored image of therapist's trajectories βx_T by applying minimal F_{PFL}. However, if the patient considers the therapist-commanded trajectories to be painful or uncomfortable for the PIL, s/he can apply enough force F_{PFL}, des, to make x_{PFL} deviate from the therapist mirrored trajectory βx_T. The PFL as a medium to convey desired trajectories from the therapist to the PIL increases the patient safety and comfort.

With the same reasoning as for (4), for the sake of closed-loop stability, the desired behavior $F_{PFL} = -F_{PFL,des}$ is replaced by an impedance surface as the desired closed-loop system at the PFL robot, through which the desired force $F_{PFL,des}$ is applied to the PFL by some modification:

$$F_{PFL} = -F_{PFL,des}(t)+ \\ M_{\vartheta,PFL} \cdot \ddot{x}_{PFL}(t) + B_{\vartheta,PFL} \cdot \dot{x}_{PFL}(t) + K_{\vartheta,PFL} \cdot x_{PFL}(t) \tag{8}$$

where $M_{\vartheta,PFL}$, $B_{\vartheta,PFL}$ and $K_{\vartheta,PFL}$ refer to the mass, damping and stiffness to be used as the local control parameters at the PFL robot. These parameters are desired to be zero for the

purpose of performance, i.e., the PFL feels $F_{PFL,des}$, entirely. However, as discussed in Section IV, setting them to non-zero values will help with stabilizing the entire closed-loop system.

C. Architecture for the therapist/robot interaction

As described earlier, in the interest of the patient's safety and comfort, the framework enables the PFL to alter the therapist-commanded trajectory, x_T, when necessary, before passing it on to the PIL. Therefore, the trajectories eventually followed by the PIL may not be exactly similar to those created by the therapist. Therefore, it is required for the therapist to receive haptic feedback about the PIL movements in relation to the therapist-commanded movements. For this purpose, position-error-based haptic feedback, $F_{\varphi,T}$, is designed to be sent to the therapist by his/her corresponding robot, as follows:

$$F_{\varphi,T}(t) = M_{\varphi,T}(\ddot{x}_{PIL}(t) - \ddot{x}_T(t))+ \\ B_{\varphi,T}(\dot{x}_{PIL}(t) - \dot{x}_T(t)) + K_{\varphi,T}(x_{PIL}(t) - x_T(t)) \tag{9}$$

where $M_{\varphi,T}$, $B_{\varphi,T}$ and $K_{\varphi,T}$ denote the mass, damping and stiffness of the position-error-based haptic feedback, respectively. With the same reasoning for (4) and (8), an impedance surface is defined for the desired closed-loop behavior at the therapist side, through which the haptic force feedback $F_{\varphi,T}$ is applied by the robot to the therapist by the modification:

$$F_T = -F_{\varphi,T}(t)+ \\ M_{\vartheta,T} \cdot \ddot{x}_T(t) + B_{\vartheta,T} \cdot \dot{x}_T(t) + K_{\vartheta,T} \cdot x_T(t) \tag{10}$$

where $M_{\vartheta,T}$, $B_{\vartheta,T}$ and $K_{\vartheta,T}$ stand for the desired mass, damping and stiffness to be used as the local control parameters at the therapist's robot. In addition, F_T refers to the force applied to the robot by the therapist. The force F_T applied by the therapist to the corresponding robot, as well as the forces F_{PIL} and F_{PFL} applied by the PIL and PFL to their corresponding robots can be modeled by second-order LTI systems [28]:

$$F_\Theta(t) = F_\Theta^*(t) - M_\Theta \cdot \ddot{x}_\Theta(t) - B_\Theta \cdot \dot{x}_\Theta(t) \\ -K_\Theta \cdot (x_\Theta(t) - x_{\Theta_0})) \tag{11}$$

where F_Θ^*, for $\Theta = PIL, PFL, T$, denote the exogenous force applied by the operator, which is either the patient or

the therapist. M_Θ, B_Θ and K_Θ stand for mass, damping and stiffness of the limb, respectively; and x_{Θ_0} indicates the initial position of the therapist's limb, x_Θ.

III. ADAPTIVE ASSIST-AS-NEEDED THERAPY

A patient-specific treatment practice that actively engages the patient in the treatment by adapting to his/her motor capability enhances the degree of recovery, compared to a non-adaptive training scenario [29], [30].

In order to promote patient active involvement, the framework provides the PIL with ANT, the level of which is decided by the GVF adjusted adaptively based on the PIL's level of impairment. In order to realize the proposed ANT strategy, objective assessment of the PIL's motor-function is essential.

A. Motor Function Assessment

By development of robotics-assisted rehabilitation, quantified evaluation of patient's motor performance and recovery has been also made possible [31], providing *objective* assessment results compared to the traditional subjective assessment approaches, e.g. Fugl Meyer [32], Motor Assessment Scale [33] and Motricity Index [34]. For this purpose, various objective and quantitative evaluation metrics have been used in the literature such as movement smoothness, movement accuracy, active range of motion, peak and mean velocity, task completion time, etc. [5], [24].

Although the above metrics provide useful quantified information about a patient's motor function, they could still be challenging, due to the intra-patient variability, to interpret and to correlate with the impairment severity of every patient regardless of their age, gender and their before-stroke baseline muscle strength. Intra-task variability is also another issue when assessing a patient's motor-function, as not every daily activity can be linked to a quantified baseline performance level. Having a baseline performance level for every single task and every single patient can be challenging, as a result of which a wide range of daily tasks cannot be included in the patient's treatment and evaluation practice.

In this paper, we take advantage of having both functional and impaired limbs of the patient involved in order to propose a novel motor function assessment metric for mirror therapy, which addresses both intra-task variability and intra-patient variability. The proposed metric, called *Performance Symmetry* can reflect the nature of any of the current metrics in the literature, but also provides a task-independent and patient-specific evaluation. In hemiparetic patients, regardless of their age, gender, baseline muscle strength, and for any type of practice tasks, the motor performance of their functional limb can reflect the ideal level of performance their impaired limb should achieve. Therefore, the performance of the PFL can be considered as the patient-specific baseline in evaluation of the PIL performance. Accordingly, unlike the absolute assessment metrics in the literature, we propose a normalized *relative* quantifying assessment metric, PS, for mirror therapy in order to provide more objective, patient-specific, and easier-to-interpret evaluation results, as follows:

$$PS_\Omega(t) = 1 - \left| \frac{\Omega_{PFL}(t) - \Omega_{PIL}(t)}{\Omega_{PFL}(t) + \Omega_{PIL}(t)} \right| \qquad (12)$$

where Ω can be any quantified metric used in conventional robotics-assisted rehabilitation. In this paper, we have used two of these metrics to incorporate in the PS assessment:

1) Movement Smoothness (MS): which is shown to be correlated with the patient's level of temporal coordination and the extent of jerky movements. Following a stroke, movements made by the affected limb are composed of sub-movements with poor temporal coordination, resulting in jerky movements. The higher the motor recovery, the smoother the movements become [24]. In order to incorporate MS into PS, it is required to calculate MS for both PFL and PIL (MS_η for $\eta = PFL$ and PIL), which can be performed as per the definition

$$MS_\eta(t) = \frac{1}{t} \int_0^t \sqrt{ \left(\frac{d^3 x_{\eta,x}}{d\tau^3} \right)^2 + \left(\frac{d^3 x_{\eta,y}}{d\tau^3} \right)^2 + \left(\frac{d^3 x_{\eta,z}}{d\tau^3} \right)^2 } \ d\tau$$
$$(13)$$

where the subscripts x, y and z refer to positions along the x, y and z directions, respectively. Calculating MS_{PFL} and MS_{PIL} based on (13), and incorporating them into (12), the movement-smoothness symmetry (PS_{MS}) will be specified as

$$PS_{MS}(t) = 1 - \left| \frac{MS_{PFL}(t) - MS_{PIL}(t)}{MS_{PFL}(t) + MS_{PIL}(t)} \right| \qquad (14)$$

This provides a normalized objective assessment of the PIL's movement smoothness without any *a priori* knowledge about the task.

2) Total Path Length (TPL): which is the total distance traveled by the patient's limb from movement onset. Comparing the TPL traveled by the PIL and the PFL gives a measure of the deviation error to indicate how accurately the PIL has been able to follow the mirrored-image of the PFL. The higher the motor recovery, the more similar the distance traveled. The total path length TPL_η for both PFL and PIL ($\eta = PFL, PIL$) can be calculated based on

$$TPL_\eta(t) = \int_0^t \sqrt{ \left(\frac{dx_{\eta,x}}{d\tau} \right)^2 + \left(\frac{dx_{\eta,y}}{d\tau} \right)^2 + \left(\frac{dx_{\eta,z}}{d\tau} \right)^2 } \ d\tau \quad (15)$$

Calculating TPL_{PIL} and TPL_{PFL} based on (15) and incorporating them into (12) gives the normalized measure of symmetry for the PIL deviation error, as follows:

$$PS_{TPL}(t) = 1 - \left| \frac{TPL_{PFL}(t) - TPL_{PIL}(t)}{TPL_{PFL}(t) + TPL_{PIL}(t)} \right| \qquad (16)$$

For any quantifying metric, the same process can be repeated to calculate the patient-specific symmetry level for that metric.

In addition to the proposed PS measure, a motor-function metric is also proposed based on the level of guidance provided to the PIL during the therapy. Most of the metrics in the literature, which are mainly meant for assessing performance, cannot distinguish in real-time whether an improved performance has been due to the patient's functional recovery or as a result of the haptic assistance guiding the patient's limb toward the practice trajectory. Therefore, we are proposing a novel metric based on the LOG provided to the PIL through the adaptive GVF during the treatment, which is beneficial in updating the quantified performance assessment based on the actual contribution and active involvement of the patient. The higher the level of guidance and assistance provided to the

PIL to accomplish the task, the lower the level of functional ability scored for the PIL. For this purpose, the normalized GVF-based LOG metric is defined as follows:

$$\psi_{GVF}(t) = 1 - \frac{\int_0^t |F_{GVF,PIL}(\tau)| \, d\tau}{|F_{GVF,max}| * t} \qquad (17)$$

where $F_{GVF,PIL}$ refers to the adaptive GVF force applied to the PIL, and $F_{GVF,max}$ indicates the maximum level of GVF force considered to apply to the PIL during a treatment session. Incorporating this metric in parallel with other performance metrics, the patient's functional improvement as well as his/her own level of contribution to the movements can be quantified.

B. Adaptive GVF Design

To incorporate the three assessment metrics PS_{MS}, PS_{TPL} and ψ_{GVF} for the purpose of updating the stiffness of the adaptive GVF applied to the PIL, given in (2), the metrics are integrated using the following fusion law:

$$\Lambda_{PIL}(t) = \frac{1}{2} \psi_{GVF}(t) * (PS_{MS}(t) + PS_{TPL}(t)) \qquad (18)$$

which combines the metrics derived based on the performance symmetry with the proposed GVF-based LOG metric in parallel, resulting in a normalized single metric between 0 and 1 to be used as an adaptive coefficient in order to update the adaptive stiffness of the GVF, $K_{GVF,PIL}$:

$$K_{GVF,PIL}(t) = \kappa_{min} + (\kappa_{max} - \kappa_{min})(1 - \Lambda_{PIL}(t)) \qquad (19)$$

where κ_{min} and κ_{max} refer to the lower and upper bounds of the GVF's stiffness, $K_{GVF,PIL}$, preset based on the level of guidance forces desired to be applied to the PIL during a treatment session. Note that having $0 \leq \Lambda_{PIL} \leq 1$ ensures that $K_{GVF,PIL}$ remains between the desired boundaries $[\kappa_{min}, \kappa_{max}]$. It should be noted that, setting $\kappa_{min} = \kappa_{max}$, would set $K_{GVF,PIL}$ to a constant value κ_{min}, which bypasses the real-time adaptation.

IV. CLOSED-LOOP STABILITY ANALYSIS

In order to satisfy the local desired closed-loop system defined for each robot as in (4), (8) and (10), a decentralized impedance controller adopted from [35] is applied. By satisfying these impedance surfaces, the closed-loop system will be decoupled in various DOFs. Therefore, stability of each DOF can be analyzed independently. By some mathematical manipulations, the proposed architecture defined in (1)-(11) can be modeled as in Fig. 3 for each DOF, and then transformed to Fig. 4 without affecting the outputs y_1 and y_2; τ_1 and τ_2 refer to communication delays from the patient to the therapist and vice versa, and

$$\Xi_1(s) = \frac{Z_{des,PFL}(s)}{Z_{\vartheta,PFL}(s) + Z_{des,PFL}(s) + Z_{PFL}(s)} \qquad (20)$$

$$\Xi_2(s) = \frac{1}{Z_{\vartheta,PIL}(s) + Z_{PIL}(s)} \qquad (21)$$

$$\Xi_3(s) = -\frac{Z_{\varphi,T}(s)}{Z_{\vartheta,T}(s) + Z_{\varphi,T}(s) + Z_T(s)} \qquad (22)$$

$$\Xi_4(s) = \frac{1}{Z_{\varphi,T}(s)} \qquad (23)$$

$$\Xi_5(s) = \frac{1}{Z_{des,PFL}(s)} \qquad (24)$$

$$\Xi_6(s) = (\Xi_1 \cdot \beta_i)^{-1} \qquad (25)$$

$$Z_{(.)}(s) = M_{(.)}s^2 + B_{(.)}s + K_{(.)}; \quad M_{(.)}, B_{(.)}, K_{(.)} > 0 \qquad (26)$$

In order to analyze the stability of the system, a combination of the Small-Gain Theorem and the Circle Criterion is applied.

Theorem I [36]: *The delayed feedback system given in Fig. 5 is Input-Output Stable (IOS) if:*

$$u_1 \in L_\infty \quad , \quad u_2 \in L_\infty \qquad (27)$$

$$\zeta_1 \in [0, \infty) \quad , \quad \zeta_2 \in [0, \infty) \qquad (28)$$

$$\zeta_1 \cdot \zeta_2 \leqslant 1 \qquad (29)$$

where, ζ_1 and ζ_2 in (28)-(29) stand for the IOS gain of subsystems Σ_1 and Σ_2, respectively, as per the following definition given for the IOS gain.

Definition I: *The IOS gain of a system with the input-output relation $y(t) = \Sigma u(t)$, where Σ is a mapping or operator that specifies y in terms of u, is a nonnegative constant ζ such that:*

$$\sup_{t \geqslant 0} |y(t)| \leqslant \zeta \cdot \sup_{t \geqslant 0} |u(t)| + \varepsilon;$$

where ε is a nonnegative constant bias term.

Therefore, in order for the closed-loop system given in Fig. 4 to remain stable, the three small-gain conditions given in (27)-(29) should be met. Based on the first condition, it is required to have

$$u_1 = F_{PFL}^\dagger + F_{PIL}^\dagger \in L_\infty \quad , \quad u_2 = F_T^\dagger \in L_\infty \qquad (30)$$

$F_T^*(t)$, $F_{PFL}^*(t)$ and $F_{PIL}^*(t)$ refer to the exogenous forces
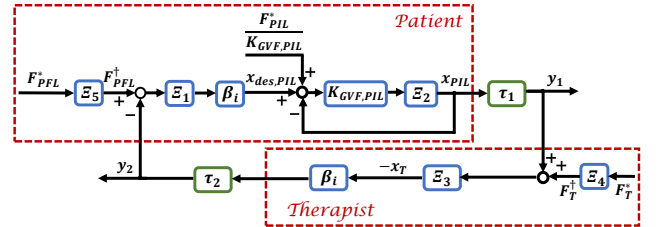
Fig. 3. The overall closed-loop system
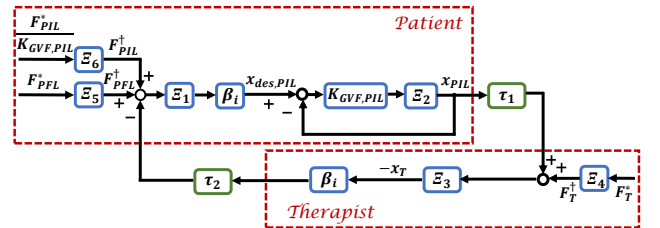
Fig. 4. The overall closed-loop system

applied by the therapist and the patient, which belong to the L_∞ space [36], while $F_T^\dagger(t)$, $F_{PFL}^\dagger(t)$ and $F_{PIL}^\dagger(t)$ indicate the outputs of the systems $\Xi_4(s)$, $\Xi_5(s)$ and $\Xi_6(s)$ for inputs $F_T^*(t)$, $F_{PFL}^*(t)$ and $\frac{F_{PIL}^*(t)}{K_{GVF,des}(t)}$, respectively. Having $0 < \kappa_{min} < K_{GVF,PIL}$ from the previous section, the input $\frac{F_{PIL}^*(t)}{K_{GVF,des}(t)}$ is also bounded and belongs to the L_∞ space. Considering the structure of systems $\Xi_4(s)$, $\Xi_5(s)$ and $\Xi_6(s)$, which are stable and proper transfer functions belonging to the L_1 space, they map inputs in L_∞ to outputs in L_∞. Consequently, $F_T^\dagger(t)$, $F_{PFL}^\dagger(t)$ and $F_{PIL}^\dagger(t)$ belong to L_∞, satisfying (27).

The next step in analyzing closed-loop stability is to check whether the IOS gains of the feedforward and the feedback paths in Fig. 4 satisfy the next two sets of conditions in (28) and (29). To calculate the IOS gain of the feedforward loop, first let us consider the local feedback loop in the feedforward path, from x_{PIL} to $x_{des,PIL}$. In this feedback loop, $K_{GVF,PIL}$ is a time-varying parameter belonging to $[\kappa_{min}, \kappa_{max}]$, as defined in the previous section. This parameter refers to the stiffness of the GVF, to be adjusted adaptively. Without the need to go into details about how to update $K_{GVF,PIL}$, it can be assumed to belong to sector $(0, \rho)$ per the following definition:

Definition II [37]: *A memoryless function* $h : [0, \infty) \times R^P \longrightarrow R^P$ *is said to belong to the sector* $(0, \rho]$ *with* $\rho = \rho^T > 0$ *if* $h(t, u)^T [h(t, u) - \rho u] \leqslant 0$.

Stability of the local feedback loop from x_{PIL} to $x_{des,PIL}$ can be analyzed using the Circle Criterion, as described next. Previously, Miandashti [38] used the Circle Criterion to study the stability of sampled-data bilateral teleoperation systems.

Theorem II [37]: *The feedback connection of a linear dynamical system* $G(s)$ *and a nonlinear element* ξ, *as shown in Fig. 6, is stable if* $\xi \in [\xi_1, \xi_2]$, *with* $\xi_2 - \xi_1 > 0$, *and* $[I + \xi_2 G(s)][I + \xi_1 G(s)]^{-1}$ *is Strictly Positive Real (SPR).*

Using a type II loop transformation [37], and considering that $\xi = K_{GVF,PIL}(t)$ is a mapping such that $K_{GVF,PIL}^{-1}$ is causal, $K_{GVF,PIL} \cdot K_{GVF,PIL}^{-1} = I$, and both $K_{GVF,PIL}$ and $K_{GVF,PIL}^{-1}$ have finite gains, the feedback connection in Fig. 6 can be transformed into the feedback system in Fig. 7. Since $0 < \kappa_{min} < K_{GVF,PIL}(t) < \kappa_{max}$, $\xi^{-1} = K_{GVF,PIL}^{-1}$ in the feedforward path of Fig. 7 does not affect the system's stability. Therefore,
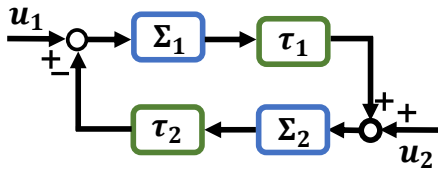
Fig. 5. Small-Gain Theorem
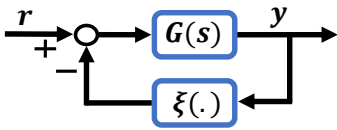
Fig. 6. Feedback connection used in the Circle Criterion

the system in Fig. 7 is identical to the feedback connection in Fig. 8 in terms of stability, which in turn is similar to that for the local feedback loop in the feedforward path, from x_{PIL} to $x_{des,PIL}$, in Fig. 4. Therefore, considering that
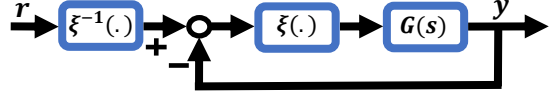
Fig. 7. Feedback connection based on the type II loop transformation [37]

$K_{GVF,PIL} \in [\kappa_{min}, \kappa_{max}]$ and based on Theorem II, the local feedback system, from x_{PIL} to $x_{des,PIL}$, in Fig. 4 is stable if $[I + \kappa_{max}\Xi_2(s)][I + \kappa_{min}\Xi_2(s)]^{-1}$ is SPR. We also need the following definitions:

Definition III [37]: *The transfer function* $H(s)$ *is SPR if* $H(s - \varepsilon)$ *if Positive Real (PR) for some* $\varepsilon > 0$.

Definition IV [37]: *The transfer function* $H(s)$ *is PR if:*

- *poles of* $H(s)$ *are in* $Re(s) < 0$
- *for all real* ω *for which* $j\omega$ *is not a pole of* $H(s)$, $H(s) + H^T(s^*)$ *is positive semi-definite, and*
- *any pure imaginary pole* $j\omega$ *of* $H(s)$ *is a simple pole and the residue* $\lim_{s \to j\omega}(s - j\omega)H(s)$ *is positive semidefinite Hermitian.*

According to Definitions III and IV, and considering the structure of $\Xi_2(s)$, which is a stable and strictly proper transfer function, $[I + \kappa_{max}\Xi_2(s)][I + \kappa_{min}\Xi_2(s)]^{-1}$ is SPR if

$$(1 + \kappa)(K_\Upsilon + \kappa_{min}) + B_\Upsilon^2 \omega^2 > (1 + \kappa)M_\Upsilon \omega^2 \quad (31)$$

where $\kappa = \kappa_{max} - \kappa_{min} > 0$, $M_\Upsilon = M_{\vartheta,PIL} + M_{PIL}$, $B_\Upsilon = B_{\vartheta,PIL} + B_{PIL}$ and $K_\Upsilon = K_{\vartheta,PIL} + K_{PIL}$. Therefore, by proper adjustment of local control parameters at the PIL side ($M_{\vartheta,PIL}$, $B_{\vartheta,PIL}$ and $K_{\vartheta,PIL}$), stability of the local feedback loop from x_{PIL} to $x_{des,PIL}$ can be guaranteed. Having the local feedback loop stable, it can be shown that the loop has its highest input-output gain when $K_{GVF,PIL}$ is at its maximum level, i.e., $K_{GVF,PIL} = \kappa_{max}$. Therefore, the IOS gain of the local feedback loop in the presence of time-varying $K_{GVF,PIL}$ will be equivalent to the IOS gain of the same loop when $K_{GVF,PIL}$ has been set to κ_{max}. Therefore, we can continue the stability analysis of the overall closed-loop system by replacing the time-varying $K_{GVF,PIL}$ by its upper bound κ_{max}, which represents the worst case. Consequently, Fig. 4 can be transformed to Fig. 9, where $\Xi_7(s) = \frac{\kappa_{max} \cdot \Xi_2(s)}{1 + \kappa_{max} \cdot \Xi_2(s)}$. Comparing Fig. 9 with Fig. 5, Σ_1 and Σ_2 can be written as

$$\Sigma_1(s) = \Xi_1(s) \cdot \beta_i \cdot \Xi_7(s) =$$
$$\frac{\beta_i \cdot \kappa_{max}}{Z_{\vartheta,PIL}(s) + Z_{PIL}(s) + \kappa_{max}} \cdot \frac{Z_{des,PFL}(s)}{Z_{\vartheta,PFL}(s) + Z_{des,PFL}(s) + Z_{PFL}(s)} \quad (32)$$

$$\Sigma_2(s) = \beta_i \cdot \Xi_3(s) = -\frac{\beta_i \cdot Z_{\varphi,T}(s)}{Z_{\vartheta,T}(s) + Z_{\varphi,T}(s) + Z_T(s)} \quad (33)$$

The next step is to investigate the condition given in (28), i.e., to have the IOS gains of $\Sigma_1(s)$ and $\Sigma_2(s)$ belong to $[0, \infty)$. Since $\Sigma_1(s)$ and $\Sigma_2(s)$ indicate transfer functions representing two LTI systems, the IOS gain is equal to the L_1 norm of the two systems; L_1 norm of transfer function $\Sigma(s)$ is
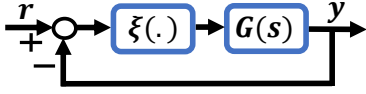
Fig. 8. Modified feedback connection used in the Circle Criterion
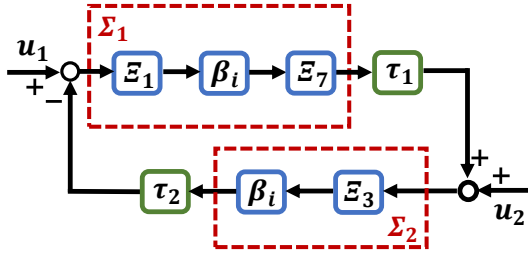
Fig. 9. The closed-loop system transformed based on the Circle Criterion

defined according to the formula $\|\Sigma(s)\|_{L_1} = \int_0^{+\infty} |\sigma(\tau)| \ d\tau$, $\sigma(t) = L^{-1}[\Sigma(s)]$. Therefore, (28) is equivalent to $\Sigma_1(s) \in L_1$ and $\Sigma_2(s) \in L_1$. Considering the structure of $\Sigma_1(s)$ and $\Sigma_2(s)$, which are stable and proper transfer functions, and knowing that β_i and κ_{max} are bounded parameters, both $\Sigma_1(s)$ and $\Sigma_2(s)$ belong to L_1. The last condition given in (29) necessitates

$$\left| \frac{\beta_i \cdot \kappa_{max}}{Z_{\vartheta,PIL}(s) + Z_{PIL}(s) + \kappa_{max}} \cdot \frac{Z_{des,PFL}(s)}{Z_{\vartheta,PFL}(s) + Z_{des,PFL}(s) + Z_{PFL}(s)} \right|_{L_1} \cdot \left| -\frac{\beta_i \cdot Z_{\varphi,T}(s)}{Z_{\vartheta,T}(s) + Z_{\varphi,T}(s) + Z_T(s)} \right|_{L_1} \leq 1 \quad (34)$$

which can be transformed into three conservative conditions, as follows:

$$\left| \frac{\beta_i \cdot \kappa_{max}}{Z_{\vartheta,PIL}(s) + Z_{PIL}(s) + \kappa_{max}} \right|_{L_1} \leq 1 \quad (35)$$

$$\left| \frac{Z_{des,PFL}(s)}{Z_{\vartheta,PFL}(s) + Z_{des,PFL}(s) + Z_{PFL}(s)} \right|_{L_1} \leq 1 \quad (36)$$

$$\left| -\frac{\beta_i \cdot Z_{\varphi,T}(s)}{Z_{\vartheta,T}(s) + Z_{\varphi,T}(s) + Z_T(s)} \right|_{L_1} \leq 1 \quad (37)$$

An approach to guarantee that (35)-(37) are satisfied is to ensure that the magnitude of each transfer function inside the brackets is not greater than one for all $s = j\omega$, i.e.,

$$|\kappa_{max}| \leq |Z_{\vartheta,PIL}(s) + Z_{PIL}(s) + \kappa_{max}| \quad (38)$$

$$|Z_{des,PFL}(s)| \leq |Z_{\vartheta,PFL}(s) + Z_{des,PFL}(s) + Z_{PFL}(s)| \quad (39)$$

$$|Z_{\varphi,T}(s)| \leq |Z_{\vartheta,T}(s) + Z_{\varphi,T}(s) + Z_T(s)| \quad (40)$$

These three inequalities along with the one given in (31) represent the stability criteria for the closed-loop system in the presence of communication time delays between the patient and the therapist. As can be seen, the control parameters $M_{\vartheta,\Delta}$, $B_{\vartheta,\Delta}$ and $K_{\vartheta,\Delta}$; $\Delta = PIL, PFL, T$ appear in all four conditions, through which the stability conditions can be satisfied.

Remark I: The proposed stability analysis platform can be applied to general *non-rehabilitation* teleoperation appli-

Quanser
HD² Haptic Device

Quanser
Rehabilitation Robots

Fig. 10. Experimental Setup

cations, as well. The framework itself can be considered as a new triple-user hierarchical/supervised leader-follower system.

V. EXPERIMENTS

In order to evaluate the performance of the proposed framework, three sets of experiments were conducted. The experimental setup consists of one Quanser HD^2 haptic device acting as the therapist's robot; and two Quanser upper-extremity rehabilitation robots serving as the PIL and PFL robots. The User Datagram Protocol (UDP) was used to transmit data between the master robots and the slave robot. All controllers and the communication between the robots were implemented using the QuaRC Real-Time system at a sampling frequency of 1 kHz. Fig. 10 shows the experimental setup.

The experiments were performed in two DOFs, along the sagittal-transverse plane. The mirroring between the PIL and the PFL was implemented across the sagittal plane. In these experiments, two operators were asked to simulate behaviors of a typical patient and a typical therapist in three distinctive scenarios in order to evaluate various features of the proposed system. The operators were familiar with the setup.

A. Scenario I: PFL-mediated Mirror Therapy

The first scenario consisted of two phases to evaluate 1) the mirroring effect between the PIL and the PFL, and 2) the impact of the PFL as a medium on the Therapist-Commanded Trajectory (TCT) received at the PIL robot. The therapist was asked to generate and repeat a squared trajectory during both phases of the experiment. The patient was asked to consider the TCT as "comfortable" in Phase I ($t = 0 - 80s$) and "uncomfortable" in Phase II ($t = 80 - 160s$), and react accordingly. Therefore, she was supposed to intentionally alter the TCT by her PFL in Phase II, where the motions were defined as "uncomfortable". A time-varying profile was set for $K_{GVF,des}$, such that $\kappa_{min} = 350$ and $\kappa_{min} = 400$. Round-trip communication delay of 200 ms was also introduced between the therapist's robot and the patient's robots.

The results are given in Figs. 11-13. Fig. 11 shows the 2D representation of the trajectories for the therapist, the PFL and the PIL. As can be seen, the therapist provided squared trajectories. The PFL followed the mirror-image of the Therapist-Commanded Trajectory (TCT), which in turn caused

the PIL to follow the TCT in the same direction, as expected. In the second phase of the experiment, where the PFL was asked to resist the TCT due to the motions being considered as "uncomfortable" for the PIL, the amplitude of the PIL motion was also reduced through the PFL-mediated architecture to avoid the painful and/or uncomfortable trajectory for the PIL. As can be seen, the framework also ensured the mirroring effect between the PIL and the PFL in both phases. Fig. 12 shows the same trajectory results in 1D, across the mirroring plan with respect to time. The force feedback provided to the therapist during the experiment is shown in Fig. 13. As can be seen, in Phase II, the therapist received considerable force on his hand informing him of the "discomfort" felt by the patient. This feature helps the therapist to be aware of and ensure the patient's safety during the therapy.
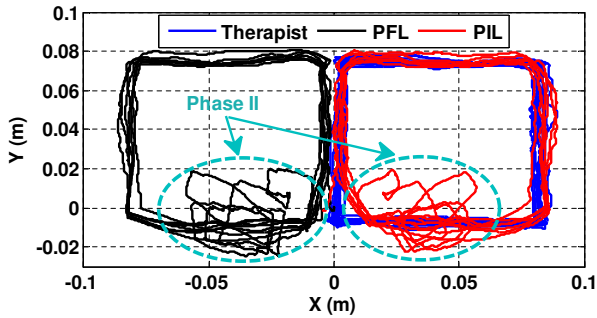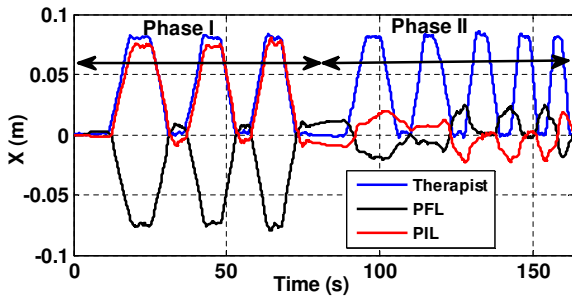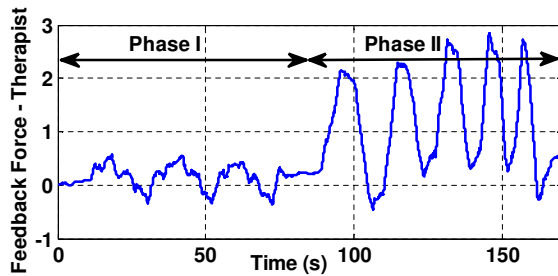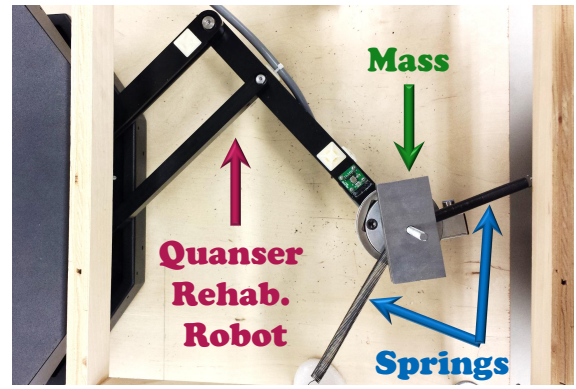
Fig. 14.   The 2-DOF mass-spring array connected to the PIL robot

B. Scenario II: How Time-Varying Assistance Helps

The second scenario was designed to investigate the effect of the time-varying virtual fixture gain $K_{GVF,des}$ on the PIL performance. For this purpose, a time-varying profile was set for $K_{GVF,des}$, increasing from $\kappa_{min} = 1$ to $\kappa_{max} = 400$ during the experiment. The round-trip communication time delay between the patient's robots and the therapist's robot was $200ms$. To simulate an impaired PIL, a 2-DOF mass-spring array was used in order to represent non-symmetric spasticity in a PIL. Spasticity, also referred to as an unusual stiffness, tightness, or pull of muscles, is a feature of altered skeletal muscle performance as a result of damage to the brain or the spinal-cord including that resulting from stroke.

For this purpose, the 2-DOF asymmetric mass-spring array was connected to the PIL robot, as shown in Fig. 14, simulating an impaired PIL affected by spasticity. Similar to the first scenario, the therapist was asked to generate squared trajectories, while the PFL was asked to consider the TCT as comfortable, thereby transferring the TCT to the PIL with no conditioning. Fig. 15 illustrates the 2-DOF time-based trajectory generated by the therapist and the trajectory followed by the simulated impaired PIL as a result of the time-varying GVF assistance force applied to the impaired PIL. As can be seen, at the beginning of the experiment, where $K_{GVF,des}$ was at its lowest value $K_{GVF,des} = \kappa_{min}$, the GVF provided minimal assistance to the PIL, thus the PIL was not able to follow the therapist-commanded trajectory. By increasing $K_{GVF,des}$ during the experiment, the level of assistance provided to the PIL increased such that during the last $50s$ of the experiment, the impaired PIL fully tracked the desired TCT.

Fig. 16 shows a 2D planar view of the same trajectories, where the smaller squares correspond to the lower levels of assistance by the GVF. As can be seen, at the beginning of the experiment, the simulated impaired PIL was not only unable to generate the desired amplitudes of the trajectory due to the low level of the GVF assistance, but also had an undesired rotational shift due to the asymmetry of the PIL. Towards the end of the experiment, increasing levels of the GVF corrected for both amplitude and rotational-shift of the trajectories. The time-varying GVF assistance enables the *adaptive* ANT in order to *actively* engage the patient in the therapy.

Fig. 11.   Experimental scenario #1: 2D plot of trajectories

Fig. 12.   Experimental scenario #1: 1D plot of trajectories across the mirroring plane

Fig. 13.   Experimental scenario #1: Haptic feedback provided to the therapist
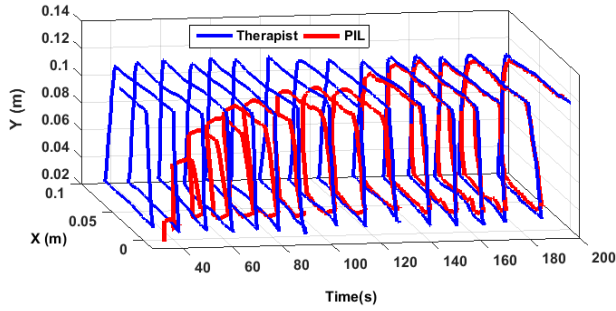
Fig. 15. Experimental scenario #2: 2D trajectories with respect to time
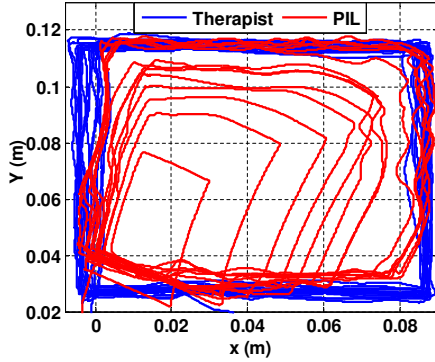
Fig. 16. Experimental scenario #2: 2D plot of trajectories

Fig. 17. Experimental scenario #3: PIL's trajectory compared with the TCT

C. Scenario III: Adaptive Patient-Targeted ANT

The third scenario was designed in three phases to evaluate various aspects of the proposed adaptive ANT strategy updated based on the patient's motor-function ability. For this purpose, the patient was asked to simulate three different motor-function levels in three Phases, as follows:

Phase I ($t = 0 - 45s$)**:** extensively impaired and unable to move. To emphasize the high level of impairment, the user was asked not to follow the PFL's mirrored movement, but to add some level of resistance to her PIL's movement (not allowing the GVF guiding her PIL along the TCT) in order to simulate a "heavy" PIL.

Phase II ($t = 45 - 85s$)**:** moderately impaired with some weakness, requiring some level of assistance from the GVF in order to complete the task.

Phase III ($t = 85 - 130s$)**:** slightly impaired, able to generate the mirror image of the PFL's movement with minimum assistance from the GVF.

The scenario's pattern can be also seen in Fig. 17, which shows a comparison between the therapist-commanded trajectory and the one made by the PIL. In phase I, the low amplitude of the PIL's movement is due to the resistance the user was asked to make to the GVF, although the GVF was trying to make her follow the TCT. In the second phase, a tracking improvement happened because the user did not resist the GVF (yet showing a moderate impairment on her PIL), enabling the GVF to assist as needed. In Phase III, the enhanced tracking was due to the ability of the PIL in following the TCT with

minimum assistance from the GVF.

The results for this experiment are given in Fig. 18-Fig. 20. Fig. 18 illustrates the proposed normalized motor-function metrics, PS_{MS}, PS_{TPL} and ψ_{GVF} (LOG), for the PIL calculated during the experiment in real-time. As can be seen, the two metrics PS_{MS} and PS_{TPL} refer to a relatively low level of motor-function for the PIL during Phase I, due to the undesirable tracking performance. The metric LOG also represents a low level of functional ability, zero at most of the time-range, as the PIL was not able to accomplish the task even with the help of the GVF; as mentioned, this phase was included to emphasize the feature of a "heavy" hand with high level of impairment, in order to provide a comparison platform for the other two phases of the experiment. In Phases II and III, the performance metrics PS_{MS} and PS_{TPL} increased considerably, which indicates the improved performance for the PIL, as expected. However, an interesting difference can be seen at the level of the functional ability shown by the metric LOG between these two phases. Although in both Phases II and III, the PIL has shown tracking improvement, the metric LOG refers to higher level of motor-function in phase III, compared to Phase II. This is a remarkable feature of the proposed LOG metric, which can distinguish between an improved performance induced by the GVF's assistance (as in Phase II) and an improvement due to the actual functional recovery of the PIL (as in Phase III).

Fig. 19 shows the adaptive stiffness of the GVF, K_{GVF} resulting from the parallel combination of the LOG with performance metrics PS_{MS} and PS_{TPL}. As can be seen, in the first phase, the system increased the K_{GVF} to its maximum level ($\kappa_{max} = 500N/m$) to assist the extensively-impaired and unable-to-move PIL. In the second phase, the stiffness was adjusted by the system to a medium level to help the moderately-impaired PIL; while in the third phase, the stiffness was reduced considerably, as the PIL's functional assessment assigned a high level of functional ability for the PIL.

Fig. 20 shows the GVF assistance provided to the PIL based on the adaptive GVF stiffness derived in accordance with the PIL's functional ability. In Phase I, the PIL was provided with a high level of GVF assistance (about 20N peak-to-peak), due to the poor motor-function. During Phase II, the GVF assistance reduced considerably (to about 9N peak-to-peak), as the PIL was able to partially perform the task and required less level of assistance. In Phase III, a slight level of GVF force was
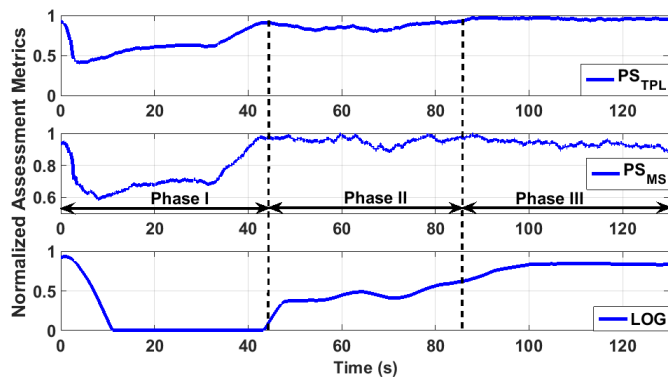
Fig. 18. Experimental scenario #3: Motor-function assessment metrics
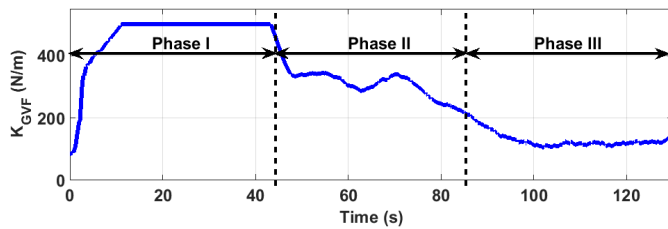
Fig. 19. Experimental scenario #3: Adaptive GVF's stiffness adjusted according to the PIL impairment level
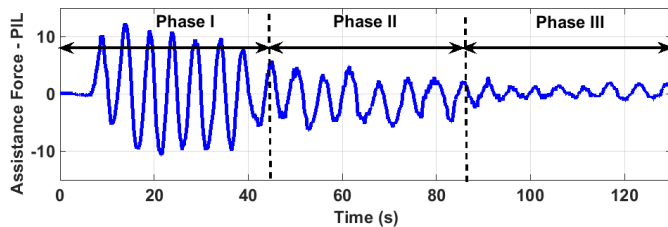
Fig. 20. Experimental scenario #3: ANT provided to the PIL

applied to the PIL (about 2N peak-to-peak), as a result of the enhanced motor-function illustrated by the PIL.

VI. CONCLUSIONS

A therapist-in-the-loop framework was presented for mirror rehabilitation therapy. Integrating an *adaptive* assist-as-needed training approach, the patient's impaired limb receives personalized therapy according to his/her level of impairment and disability. This enables the patient's impaired limb to be *actively* involved in the therapy. The expectation is that this will play an important role in promoting functional recovery and motor learning, as opposed to moving passively. Using the proposed framework, the desired therapy trajectories are transferred from the therapist to the patient's impaired limb after being conditioned by the patient's functional limb especially when trajectories that are painful or uncomfortable for the impaired limb are prescribed by the therapist. In order to inform the therapist about any discomfort at the patient's side causing the desired trajectories to alter, haptic feedback from the patient's impaired limb is provided to the therapist. A criterion was also designed for updating the adaptive ANT implemented by the guidance virtual fixture, based on the patient's impairment

level. Two assessment metrics, Performance Symmetry (PS) and Level Of Guidance (LOG), were developed to facilitate the patient-targeted therapy and evaluation. Stability of the closed-loop system was investigated using a combination of the Circle Criterion and the Small-Gain Theorem. The stability analysis took into account the *adaptive* assist-as-needed therapy as well as communication time-delays between the patient and the therapist, facilitating tele/in-home rehabilitation applications. The proposed stability analysis platform can be possibly applied to general non-rehabilitation teleoperation applications, as well. Experimental results were reported to show the performance of the proposed framework.

Our future work will focus on conducting clinical trials in order to evaluate the effectiveness of the proposed framework in real scenarios. Two interesting aspects to investigate are the effect of patients' gender and their limb dominance on the efficacy of the therapy provided through the proposed framework. As discussed in the literature, gender may affect the outcome of the therapy [39]. Limb dominance may also have some effect on the level of skills acquisition as a result of specific brain activation patterns or the amount of limb use during regular activities [40].

REFERENCES

[1] http://www.strokecenter.org/patients/about-stroke/stroke-statistics/. [Online]. Available: http://www.strokecenter.org/patients/about-stroke/stroke-statistics/

[2] A. Otten *et al.*, "Limpact: A hydraulically powered self-aligning upper limb exoskeleton," *IEEE/ASME Transactions on Mechatronics*, vol. 20, no. 5, pp. 2285–2298, 2015.

[3] B. B. Johansson, "Brain plasticity and stroke rehabilitation the willis lecture," *Stroke*, vol. 31, no. 1, pp. 223–230, 2000.

[4] H. I. Krebs *et al.*, "Robot-aided neurorehabilitation," *IEEE Transactions on Rehabilitation Engineering*, vol. 6, no. 1, pp. 75–87, 1998.

[5] R. Colombo *et al.*, "Robotic techniques for upper limb evaluation and rehabilitation of stroke patients," *IEEE Transactions on Neural Systems and Rehabilitation Eng.*, vol. 13, no. 3, pp. 311–324, 2005.

[6] S. Hesse *et al.*, "Robot-assisted arm trainer for the passive and active practice of bilateral forearm and wrist movements in hemiparetic subjects," *Archives of physical medicine and rehabilitation*, vol. 84, no. 6, pp. 915–920, 2003.

[7] H. I. Krebs and N. Hogan, "Therapeutic robotics: A technology push," *Proceedings of the IEEE*, vol. 94, no. 9, pp. 1727–1738, 2006.

[8] http://www.stroke.org/site/pageserver?pagename=hemiparesis. [Online]. Available: http://www.stroke.org/site/PageServer?pagename=hemiparesis

[9] C. Dohle *et al.*, "Mirror therapy promotes recovery from severe hemiparesis: a randomized controlled trial," *Neurorehabilitation and neural repair*, vol. 23, no. 3, pp. 209–217, 2009.

[10] A. Parton *et al.*, "Hemispatial neglect," *J. of Neurology, Neurosurgery & Psychiatry*, vol. 75, no. 1, pp. 13–21, 2004.

[11] H. Kim *et al.*, "Kinematic data analysis for post-stroke patients following bilateral versus unilateral rehabilitation with an upper limb wearable robotic system," *IEEE Transactions on Neural Systems and Rehabilitation Engineering*, vol. 21, no. 2, pp. 153–164, 2013.

[12] A. R. Luft *et al.*, "Repetitive bilateral arm training and motor cortex activation in chronic stroke: a randomized controlled trial," *The J. of the American Med. Association*, vol. 292, no. 15, pp. 1853–1861, 2004.

[13] M. E. Michielsen *et al.*, "The neuronal correlates of mirror therapy: an fMRI study on mirror induced visual illusions in patients with stroke," *J. of Neurol., Neurosurg. & Psychiat.*, vol. 82, no. 4, pp. 393–398, 2011.

[14] J. H. Cauraugh and J. J. Summers, "Neural plasticity and bilateral movements: a rehabilitation approach for chronic stroke," *Progress in neurobiology*, vol. 75, no. 5, pp. 309–320, 2005.

[15] J. J. Summers *et al.*, "Bilateral and unilateral movement training on upper limb function in chronic stroke patients: a TMS study," *Journal of the neurological sciences*, vol. 252, no. 1, pp. 76–82, 2007.

[16] E. L. Altschuler *et al.*, "Rehabilitation of hemiparesis after stroke with a mirror," *The Lancet*, vol. 353, no. 9169, pp. 2035–2036, 1999.

[17] J. A. Stevens and M. E. P. Stoykov, "Using motor imagery in the rehabilitation of hemiparesis," *Archives of physical medicine and rehabilitation*, vol. 84, no. 7, pp. 1090–1092, 2003.

[18] J. A. Stevens and M. E. P. Stoykov, "Simulation of bilateral movement training through mirror reflection: a case report demonstrating an occupational therapy technique for hemiparesis," *Topics in stroke rehabilitation*, vol. 11, no. 1, pp. 59–66, 2004.

[19] K. Sathian *et al.*, "Doing it with mirrors: a case study of a novel approach to neurorehabilitation," *Neurorehabilitation and Neural Repair*, vol. 14, no. 1, pp. 73–76, 2000.

[20] P. Lum *et al.*, "The mime robotic system for upper-limb neurorehabilitation: results from a clinical trial in subacute stroke," in *9th International Conf. on Rehabilitation Robotics*, 2005, pp. 511–514.

[21] M. Shahbazi *et al.*, "Novel cooperative teleoperation framework: Multi-master/single-slave system," *IEEE/ASME Transactions on Mechatronics*, vol. 20, no. 4, pp. 1668–1679, 2015.

[22] G. Ganesh *et al.*, "Two is better than one: Physical interactions improve motor performance in humans," *Scientific reports, Nature Pub. Group*, vol. 4, 2014.

[23] R. Prada and S. Payandeh, "A study on design and analysis of virtual fixtures for cutting in training environments," in *First Joint Eurohaptics Conference and Symposium on Haptic Interfaces for Virtual Environment and Teleoperator Systems, World Haptics*, 2005, pp. 375–380.

[24] B. Rohrer *et al.*, "Movement smoothness changes during stroke recovery," *The J. of Neuroscience*, vol. 22, no. 18, pp. 8297–8304, 2002.

[25] C. R. Carignan and H. I. Krebs, "Telerehabilitation robotics: bright lights, big future?" *Journal of rehabilitation research and development*, vol. 43, no. 5, p. 695, 2006.

[26] S. F. Atashzar *et al.*, "Networked teleoperation with non-passive environment: Application to tele-rehabilitation," in *IEEE/RSJ International Conference on Intelligent Robots and Systems*, 2012, pp. 5125–5130.

[27] A. Haddadi *et al.*, "Operator dynamics consideration for less conservative coupled stability condition in bilateral teleoperation," *IEEE/ASME Transactions on Mechatronics*, vol. 20, no. 5, pp. 2463–2475, 2015.

[28] M. Dyck and M. Tavakoli, "Measuring the dynamic impedance of the human arm without a force sensor," in *Int. Conf. Rehab. Robotics*, 2013.

[29] N. Hogan *et al.*, "Motions or muscles? some behavioral factors underlying robotic assistance of motor recovery," *Journal of rehabilitation research and development*, vol. 43, no. 5, p. 605, 2006.

[30] M. Ferraro *et al.*, "Robot-aided sensorimotor arm training improves outcome in patients with chronic stroke," *Neurology*, vol. 61, no. 11, pp. 1604–1607, 2003.

[31] A. U. Pehlivan *et al.*, "A subject-adaptive controller for wrist robotic rehabilitation," *IEEE/ASME Transactions on Mechatronics*, vol. 20, no. 3, pp. 1338–1350, 2015.

[32] A. R. Fugl-Meyer *et al.*, "The post-stroke hemiplegic patient. 1. a method for evaluation of physical performance." *Scandinavian journal of rehabilitation medicine*, vol. 7, no. 1, pp. 13–31, 1974.

[33] J. H. Carr *et al.*, "Investigation of a new motor assessment scale for stroke patients," *Physical therapy*, vol. 65, no. 2, pp. 175–180, 1985.

[34] C. Collin and D. Wade, "Assessing motor impairment after stroke: a pilot reliability study." *Journal of Neurology, Neurosurgery & Psychiatry*, vol. 53, no. 7, pp. 576–579, 1990.

[35] M. Shahbazi *et al.*, "A novel shared structure for dual user systems with unknown time-delay utilizing adaptive impedance control," in *2011 IEEE Int. Conf. on Robotics and Automation*, 2011, pp. 2124–2129.

[36] I. Polushin *et al.*, "A multichannel IOS small gain theorem for systems with multiple time-varying communication delays," *IEEE Transactions on Automatic Control*, vol. 54, no. 2, pp. 404–409, 2009.

[37] H. K. Khalil and J. Grizzle, *Nonlinear systems*. Prentice Hall, Upper Saddle River, 2002, vol. 3.

[38] N. Miandashti and M. Tavakoli, "Stability of sampled-data, delayed haptic interaction and teleoperation," in *2014 IEEE Haptics Symposium*, 2014, pp. 215–220.

[39] M.-F. Kuo *et al.*, "Sex differences in cortical neuroplasticity in humans," *Neuroreport*, vol. 17, no. 16, pp. 1703–1707, 2006.

[40] R. Lima *et al.*, "Influences of hand dominance on the maintenance of benefits after home-based modified constraint-induced movement therapy in individuals with stroke," *Brazilian journal of physical therapy*, vol. 18, no. 5, pp. 435–444, 2014.